Article

Analysis of Pre-Earthquake Ionospheric Anomalies in the Japanese Region Based on DEMETER Satellite Data

Jingming Lu [1], Yaogai Hu [1,*], Chunhua Jiang [1], Zhengyu Zhao [1], Yuannong Zhang [1] and Zhengzheng Ma [2]

[1] School of Electronic Information, Wuhan University, Wuhan 430079, China; jingminglu@whu.edu.cn (J.L.); chuajiang@whu.edu.cn (C.J.); zhaozy@whu.edu.cn (Z.Z.); ynzhang@whu.edu.cn (Y.Z.)

[2] China Research Institute of Radiowave Propagation, Qingdao 266107, China; mazz@crirp.ac.cn

* Correspondence: yaogaihu@whu.edu.cn

Abstract: The electron density (N_e), ion density (N_i), and electron temperature (T_e) statistics recorded by the DEMETER satellite payload ISL (Instrument Sonde de Langmuir) were used to study the disturbance characteristics of the ionosphere before solid earthquakes of magnitude 6 or higher in Japan during the summer of 2005–2009, to provide more information and methods for the coupling mechanism and short-range earthquake prediction. In this paper, the region of $\pm10°$ of the epicenter is divided into $1° \times 1°$ pixels, and the background field of each parameter is constructed using data without earthquakes and relatively calm space weather. We also define a measure of the perturbation intensity of ionospheric parameters relative to the background field during the occurrence of earthquakes. The analysis results of the four Japanese earthquakes from space and time show an excellent synchronization in the time and area of the anomalies in ionospheric parameters of the four cases. All four instances showed N_e abnormalities, and three showed N_i and T_e anomalies, in which N_e and N_i increased or decreased abnormally, while T_e increased abnormally every time, and the anomalies mainly occurred about 9–12 days before the earthquake. This paper eliminates the influence of solar, geomagnetic, and satellite data defects on the experimental results as much as possible in data screening and method selection. The results partially agree with the conclusions reported in the existing literature, and the obtained anomalies are somewhat related to the ionospheric precursors of earthquakes.

Keywords: DEMETER satellite; electron density; ion density; electron temperature; seismic ionospheric precursor

1. Introduction

More and more, research results show that the impact of earthquakes on the earth's environment is not only limited to the Earth's surface but may also affect the upper atmosphere and ionosphere, causing anomalies in ionospheric electron concentrations and other parameters. With the development of space exploration technology, ionospheric anomalies are receiving more and more attention as a new type of short-range precursor of earthquakes, and there are already articles showing that strong ionospheric disturbances or anomalies occur before strong earthquakes [1–4].

France launched the DEMETER satellite, the first satellite to provide data for studying ionospheric disturbance information related to earthquakes [5]. Parrot used DEMETER satellite data to repeatedly study the perturbation of electromagnetic waves and ionospheric parameters overhead before the earthquake [6]. Zeng found a sharp change of >20% in N_e and T_e near the epicenter 4 and 5 days before the Wenchuan earthquake [7]. Ouyang found that the earthquake causes a synchronous increase in N_e and O^+ density [8]. Zhang used DEMETER satellite payload ICE (Instrument Champ Electrique) [9] data to find electrostatic perturbations in the ULF and ELF bands before the earthquake [10]. Yan found that anomalous disturbances of N_e were more easily captured in the seismic

region at $\pm 20°$ equatorial latitude [5]. Yan found that anomalous ionospheric perturbations associated with earthquakes of magnitude greater than 5 were evident at night, and that perturbations in N_i were also observed close to the epicenter after the earthquake [11]. Li mentioned that the sensitivity of N_i to seismic activity tends to be higher than that of N_e [12]. Zheng found that the apparent extent and intensity of ionospheric anomalies increased with increasing magnitude and that post-earthquake ionospheric disturbances were very pronounced [13]. There are many domestic and international studies on the DEMETER satellite, but there are few reports on using it to study pre-earthquake ionospheric anomalies in the Japanese region. Japan is in the earthquake-prone Pacific Rim seismic zone, which is well suited for a statistical study of the changes in ionospheric parameters over earthquakes before multiple strong earthquakes in the same region.

In this paper, the background fields of mean and standard deviation of three ionospheric parameters (N_e, N_i, and T_e) were first constructed. Then the ionospheric parameter values of strong earthquakes in Japan from 2005 to 2009 were compared with the background values to obtain the general pattern of ionospheric anomalies in the region before the earthquakes.

2. Data and Shock Example Screening

All publicly available data from the DEMETER satellite can be downloaded from the official website of the French Data Center for Plasma Physics (CDPP: Centre de données de la Physique des Plasmas). This paper uses data from the payload ISL (Instrument Sonde de Langmuir) [14], which contains two types of data, 1143 and 1144, corresponding to plasma parameter data recorded by the satellite in the survey and burst modes, respectively. This paper combines the two data types to form complete orbital data for analyzing ionospheric anomaly information. The screening of ISL payload data is mainly considered from the following two aspects: (1) Since the DEMETER satellite will have missing orbits and data loss in the second half of the service period starting from 2004 and the first half of the retirement period in 2010, and the ionosphere in the mid-latitude area is more sensitive to seasonal changes, this paper mainly uses ionospheric data from the DEMETER satellite ISL payload during the summer period of 2005–2009 (May, June, July, and August) for the study; (2) To avoid the influence of magnetic storms on the experimental results, according to the geomagnetic indices (Dst and Kp), the data under complex space weather with $Dst \leq -30$ nT and $Kp \geq 3$ are excluded. In addition, since the solar influence on the ionosphere at night is smaller compared to daytime, nighttime data are more suitable for capturing ionospheric anomalies related to earthquakes, and only nighttime data are used in this paper for the study.

According to the earthquake catalog on the official website of the China Earthquake Administration (https://www.cea.gov.cn/cea/index/index.html) (accessed on 24 December 2020), several significant earthquakes occurred in the selected area of Japan during the summer of 2005–2009, and the earthquake example information is shown in Table 1.

Table 1. Information on earthquakes.

Earthquake Number	Date	Epicenter	Magnitude	Depth/km	Space Range		Time Range	
					Latitude	Longitude	Start Date	End Date
1	16 July 2007	36.7° N, 135.2° E	6.9	350	27–47° N	125–145° E	1 July 2007	16 July 2007
	8 May 2008	36.1° N, 141.6° E	7.1	10				
2	14 June 2008	39.1° N, 140.8° E	7.0	10	29–49° N	131–151° E	30 May 2008	14 June 2008
3	19 July 2008	37.5° N, 142.3° E	7.3	10	27–47° N	132–152° E	4 July 2008	19 July 2008

| 4 | 9 August 2009 | 33.1° N, 138.2° E | 7.2 | 10 | 23–43° N | 128–148° E | 25 July 2009 | 9 August 2009 |
| | 13 August 2009 | 32.6° N, 140.5° E | 6.5 | 96 | | | | |

3. Analysis Process

It has been shown that the ionospheric anomalies caused by earthquakes in the gestation process do not necessarily occur over the epicenter but within the gestation zone, and the extent of the gestation zone expands with the increase in magnitude [15,16].

According to the formula for estimating the size of the lithospheric gestation zone proposed by Dobrovolsky [17]:

$$R = 10^{0.43M},\tag{1}$$

where R is the diameter of the gestation zone in km and M is the earthquake magnitude, the maximum radius of the gestation zone of the earthquake case studied in this paper is about 1377 km (magnitude 7.3). Assuming that the epicenter latitude and longitude are $(LAT0, LONG0)$, the size of the study area is selected as $(LAT0 \pm 10°, LONG0 \pm 10°)$, and the pixel size is set to $1° \times 1°$. Since the ionospheric anomalies are short-lived in time, this paper selects 15 days before the earthquake plus the day of the earthquake as a set of data for studying ionospheric anomalies from the filtered data.

Taking the 6.9 magnitude earthquake (epicenter: 36.7° N, 135.2° E) that occurred in Japan on 16 July 2007, as an example, the parameter N_e is used to illustrate the research method of this paper. First, the statistical background field of the observed parameter N_e is constructed. The study area is $(37° N \pm 10°, 135° E \pm 10°)$ and is divided into 400 pixels. The background data are allocated to the corresponding pixels according to the latitude and longitude, and the mean and standard deviation of the data in each pixel are obtained, and 20 × 20 mean matrix β (Figure 1a) and standard deviation matrix σ (Figure 1b) are obtained. Next, the variation field of the observed parameters of the seismic data is constructed. The seismic data are selected from the day of the earthquake and the fifteen days before the earthquake(from 1 July 2007 to 16 July 2007), and only the mean values of the data in each pixel are obtained to obtain a set of 20 × 20 seismic data mean matrices α (Figure 1c). Finally, define the disturbance intensity indicator t.

$$t = \frac{|\alpha - \beta|}{\sigma},\tag{2}$$

The *t*-value of the data in each pixel is calculated using Equation (2). The calculated results are mapped as color indicators plotted in Figure 1d. In this paper, the process of obtaining t using Equation (2) is referred to as the normalization process of the ionospheric parameter values of the seismic data with respect to the background data. The magnitude of the obtained t-value can measure the intensity of the perturbation of the seismic data to the background field data, and t is a dimensionless indicator. According to the 3σ criterion in statistics, when the magnitude of the parameter t exceeds 3, an ionospheric anomaly is considered to have occurred in the region before the earthquake. The pentagram in Figure 1 indicates the epicenter, and the small black dots in Figure 1c,d show the trajectory of the satellite. The same symbols in the following figures represent the same meaning.
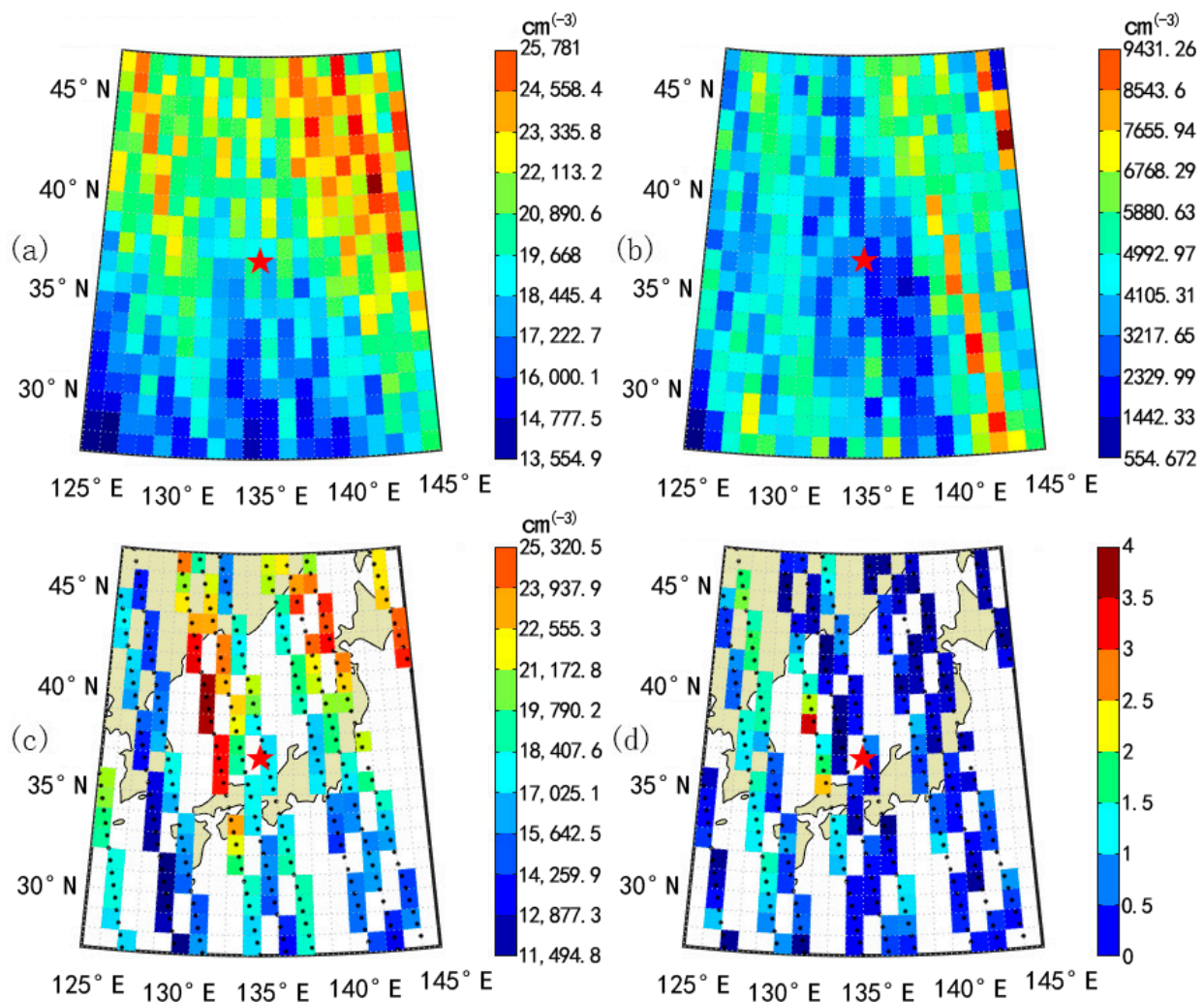
Figure 1. (**a**) Background mean plot of parameter N_e; (**b**) Background standard deviation plot of parameter N_e; (**c**) Mean plot of seismic data of parameter N_e of earthquake case on 16 July 2007; (**d**) Normalized result plot of parameter N_e of earthquake case on 16 July 2007.

4. Analysis Results and Discussion

4.1. Construction of Background Fields and Seismic-Free Comparison Tests

Background fields were constructed for each of the three ionospheric parameters N_e, N_i, and T_e in the ISL load, as shown in Figure 2. It is evident from the mean background fields Figure 2a–c that T_e increases with increasing latitude. This pattern of increase with latitude for N_e and N_i is relatively weak, but there is still this regular trend, which is partly consistent with the regularity found by Wang [18] when checking the consistency of ISL ion density data. The overall variation of N_e and T_e is smoother compared to N_i, as seen in the standard deviation background fields Figure 2d–f.
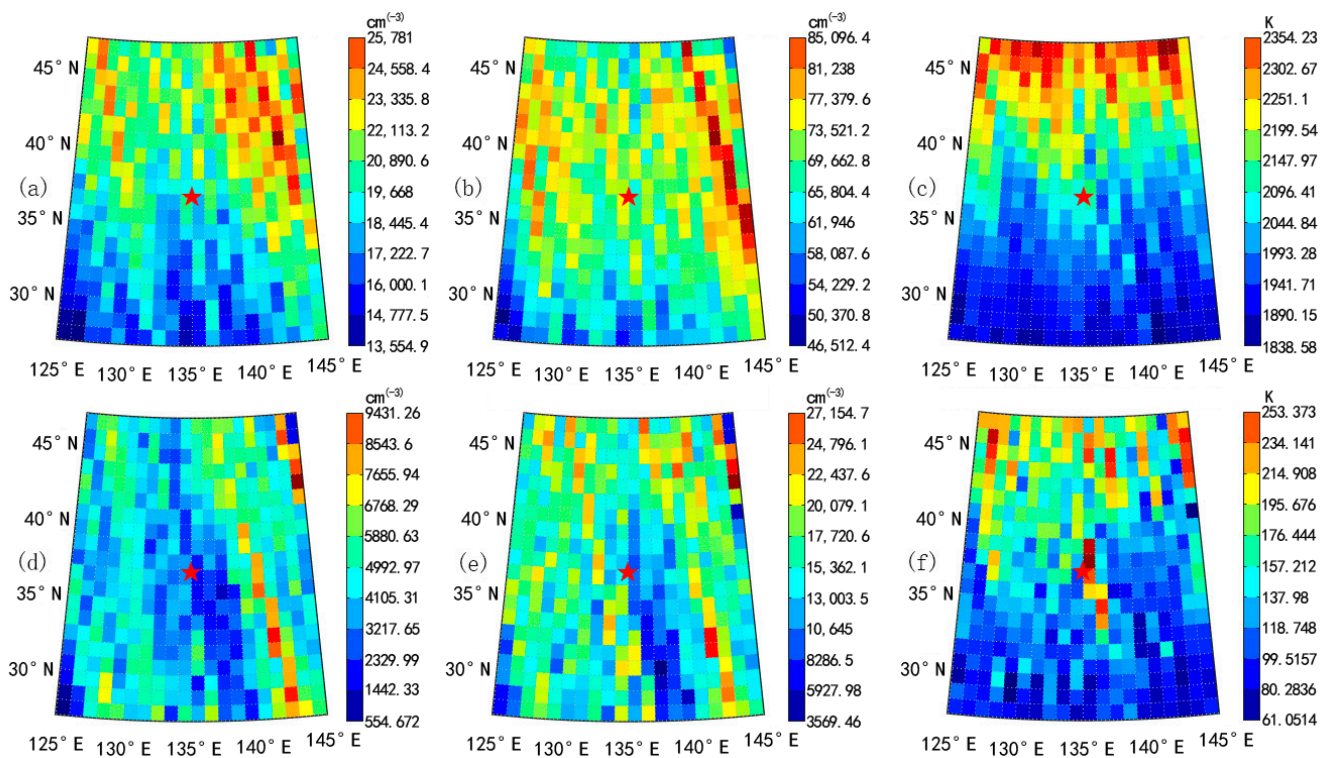
Figure 2. (**a**) Background mean plot of parameter N_e; (**b**) Background mean plot of parameter N_i; (**c**) Background mean plot of parameter T_e; (**d**) Background standard deviation plot of parameter N_e; (**e**) Background standard deviation plot of parameter N_i; (**f**) Background standard deviation plot of parameter T_e.

To make the anomalous results more objective, the data during the no-earthquake period were divided into 15-day groups and normalized to the background data to obtain the variation of the disturbance intensity index t under the no-earthquake and geomagnetically calm conditions (after data filtering, 15 days of data needs more days to be satisfied, so the time interval in Figure 3 is greater than 15 days). The results of the background data for 2005 are shown in Figure 3. From Figure 3, we can see that the indicator t does not exceed 3 under the no-earthquake condition and the relatively calm space weather condition. A pixel is randomly selected from Figure 3 to plot a time series of three parameters, as shown in Figure 4. As can be seen in Figure 4, the three parameters without a seismic case also have no anomalies over 3 in the time series, and the overall variation of N_e and N_i is relatively consistent. To better understand the correlation degree between the parameters, the background data are assigned to 400 pixels in this paper, and then the correlations between the parameters in each grid are counted and plotted as in Figure 5. The red line in Figure 5 indicates that the Pearson correlation coefficient is 0.7, from which it can be seen that the correlations of N_e and N_i mostly lie on 0.7, showing a strong positive correlation.
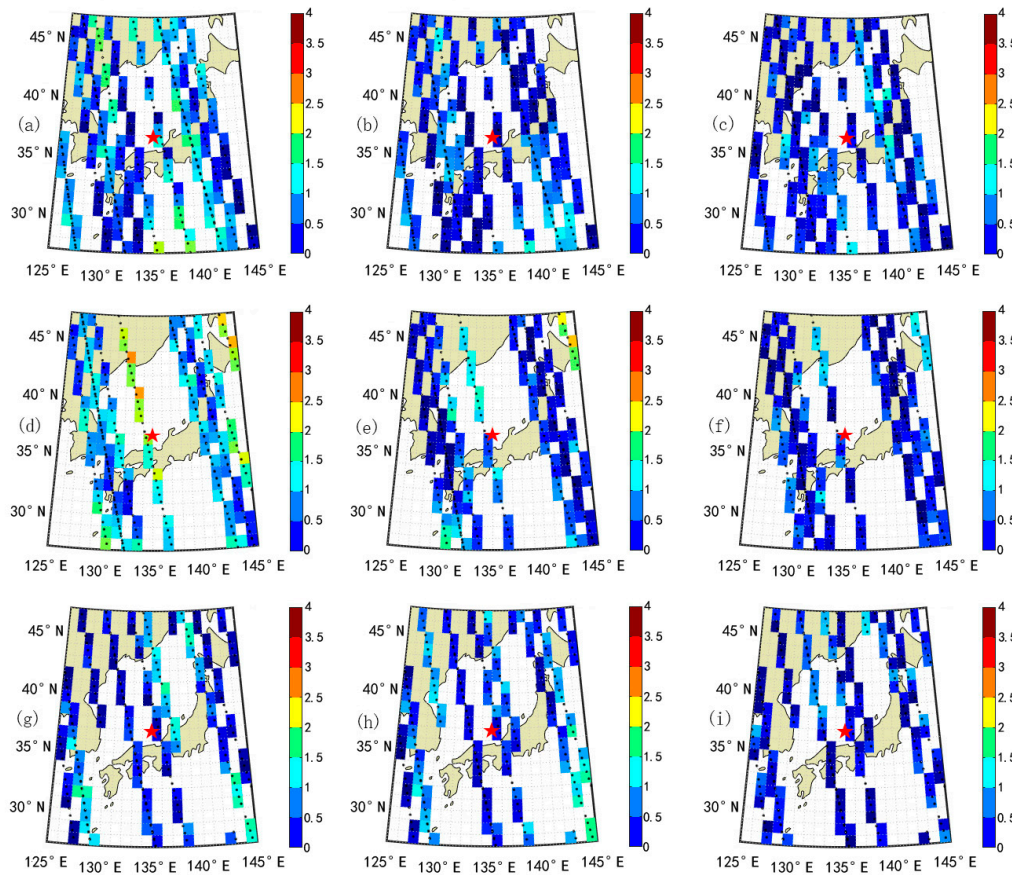
Figure 3. (**a**) Normalized result plot of parameter N_e from 2 May 2005 to 10 June 2005; (**b**) Normalized result plot of parameter N_i from 2 May 2005 to 10 June 2005; (**c**) Normalized result plot of parameter T_e from 2 May 2005 to 10 June 2005; (**d**) Normalized result plot of parameter N_e from 11 June 2005 to 19 July 2005; (**e**) Normalized result plot of parameter N_i from 11 June 2005 to 19 July 2005; (**f**) Normalized result plot of parameter T_e from 11 June 2005 to 19 July 2005; (**g**) Normalized result plot of parameter N_e from 20 July 2005 to 30 August 2005; (**h**) Normalized result plot of parameter N_i from 20 July 2005 to 30 August 2005; (**i**) Normalized result plot of parameter T_e from 20 July 2005 to 30 August 2005.
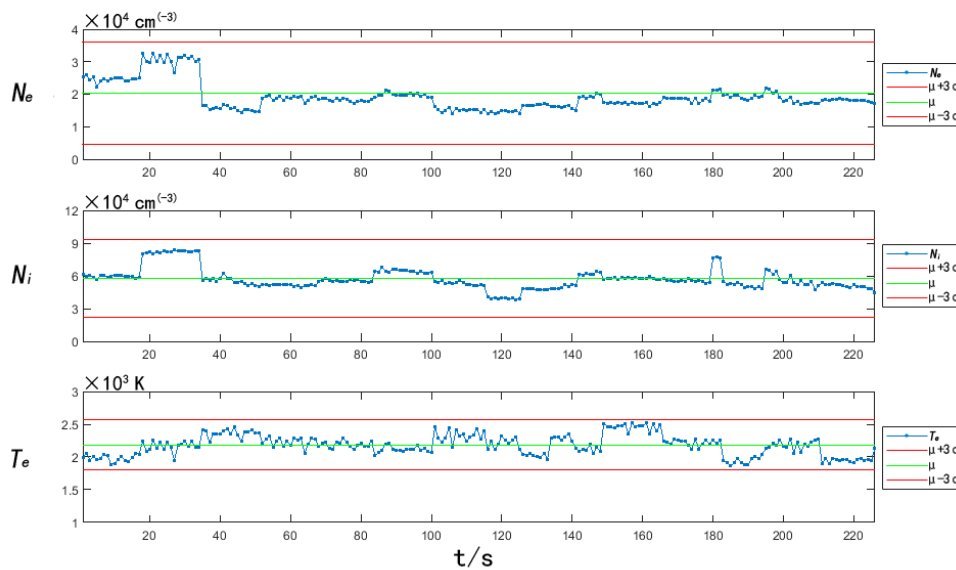

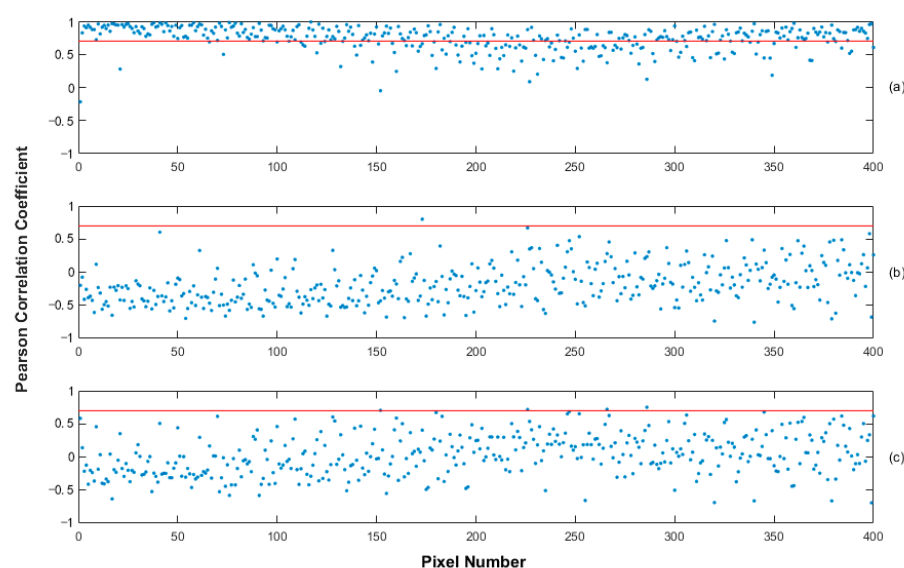**Figure 4.** Three-parameter time series without earthquake occurrence.

Figure 5. (**a**) Statistical plot of correlation coefficients of N_e and N_i; (**b**) Statistical plot of correlation coefficients of N_e and T_e; (**c**) Statistical plot of correlation coefficients of N_i and T_e.

4.2. Earthquake Example 1

The filtered seismic data are normalized to the background field according to Equation (1) for each of the three parameters, and the results are shown in Figure 6. In Figure 6, the pixels with more than 3 anomalies have been circled with red circles and numbered sequentially, and the information of each anomaly region is shown in Table 2. The selected abnormal pixels are marked with red circles and numbers in the subsequent normalized result plots.
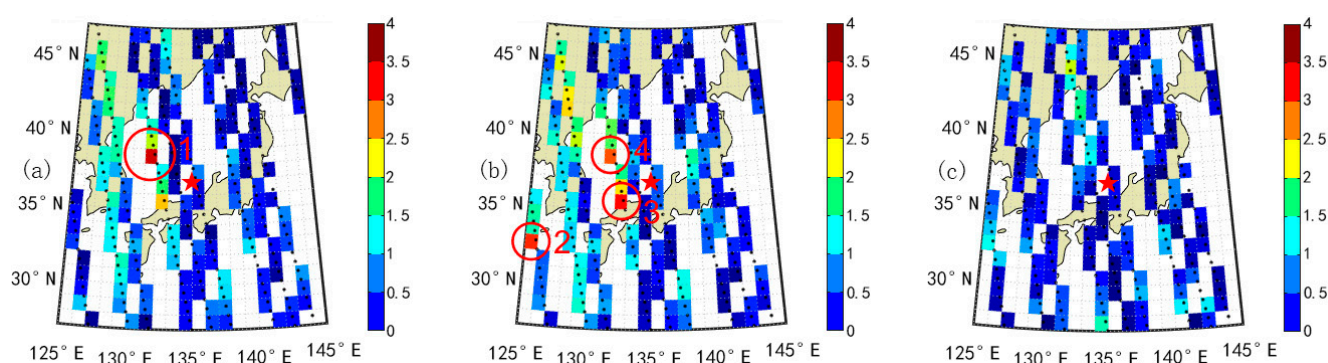

Figure 6. (**a**) Normalized results plot of parameter N_e of earthquake case on 16 July 2007; (**b**) Normalized results plot of parameter N_i of earthquake case on 16 July 2007; (**c**) Normalized results plot of parameter T_e of earthquake case on 16 July 2007.

Table 2. Earthquake case 16 July 2007 anomalous area information.

Region Number	Space Range		Corresponding Orbit	Corresponding Date
	Latitude	Longitude		
1	38–39° N	131–132° E	16070_1	6 July 2007
2	32–33° N	125–126° E	16085_1	7 July 2007
3	35–36° N	132–133° E	16070_1	6 July 2007
4	38–39° N	131–132° E	16070_1	6 July 2007

Figures 7–9 show the curves of the three parameters in the anomalous regions 1, 2, and 3 with time, respectively. From Figures 7–9, it can be seen that N_e and N_i showed synchronous anomalous enhancement on the tenth day before the earthquake (6 July 2007); N_i showed anomalous enhancement on the ninth day before the earthquake (7 July 2007), and the magnitude of N_e enhancement was not apparent. Comparing these three time-varying graphs shows that the timing of the anomalies in N_e and N_i is more synchronized. Comparing Figures 3 and 4, it can be concluded that these anomalies may be spatially and temporally related to the current earthquake case. The T_e anomaly was not captured in this seismic case study.
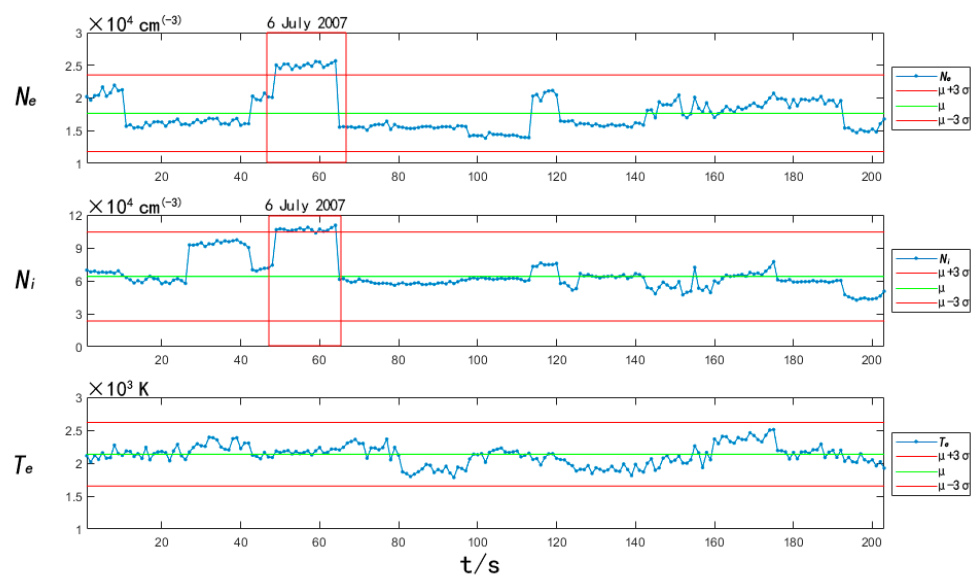

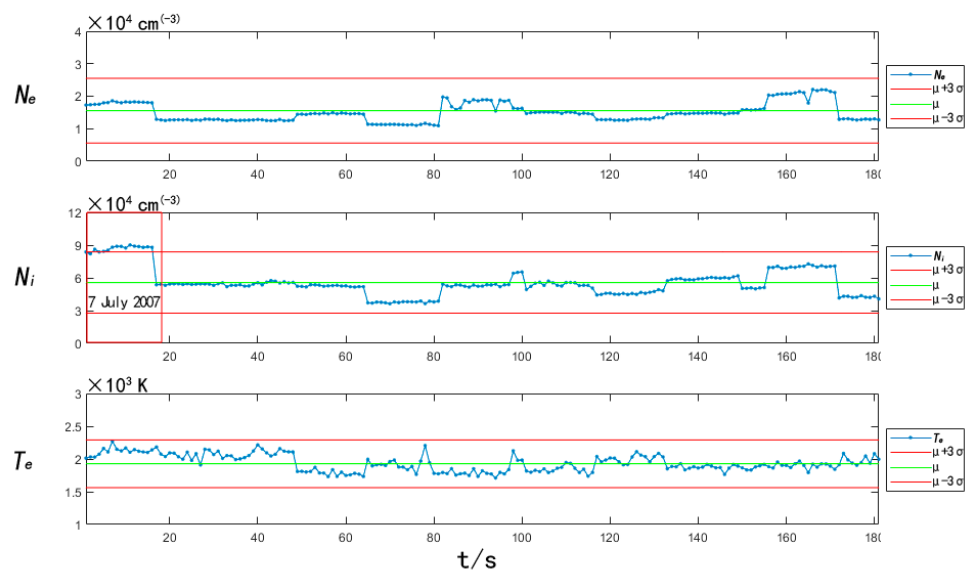**Figure 7.** Three-parameter time series plot within anomaly region 1 in seismic example 1.

Figure 8. Three-parameter time series plot within anomaly region 2 in seismic example 1.
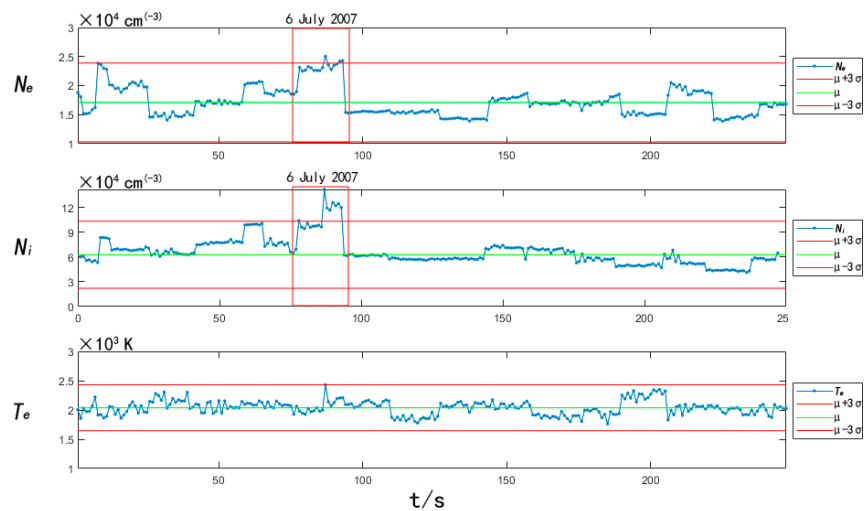
Figure 9. Three-parameter time series plot within anomaly region 3 in seismic example 1.

4.3. Earthquake Example 2

The normalized results of the same processing for this earthquake example are shown in Figure 10. Considering that anomalies in the same region of the same track have the same manifestation, for region 1 in Figure 10a, the results of only one pixel are selected to represent the whole region 1. The information on the anomalous regions selected for this earthquake example is shown in Table 3.
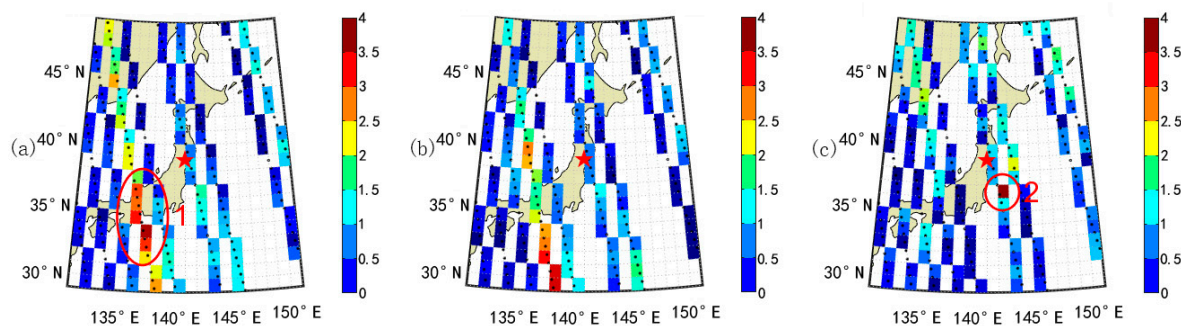

Figure 10. (**a**) Normalized results plot of parameter N_e of earthquake case on 14 June 2008; (**b**) Normalized results plot of parameter N_i of earthquake case on 14 June 2008; (**c**) Normalized results plot of parameter T_e of earthquake case on 14 June 2008.

Table 3. Earthquake case 14 June 2008 anomalous area information.

Region Number	Space Range		Corresponding Orbit	Corresponding Date
	Latitude	Longitude		
1	32–33° N	137–138° E	20946_1	2 June 2008
2	36–37° N	142–143° E	21078_1	11 June 2008

Figures 11 and 12 show the curves of the three parameters within the anomalous regions 1 and 2 with time, respectively. By combining Figures 10 and 11, it can be seen that a simultaneous anomalous weakening of N_e and N_i occurred southwest of the epicenter on the twelfth day before the earthquake (2 June 2008). Compared to Figure 3, it can be analyzed that this anomalous weakening phenomenon is closely related to this earthquake example in both time and space dimensions. Combining Figures 10 and 12, it can be seen that on the third day before the earthquake (11 June 2008), T_e showed an

anomalous strengthening in the southeast direction of the epicenter, while N_e and N_i did not show anomalies at this time.
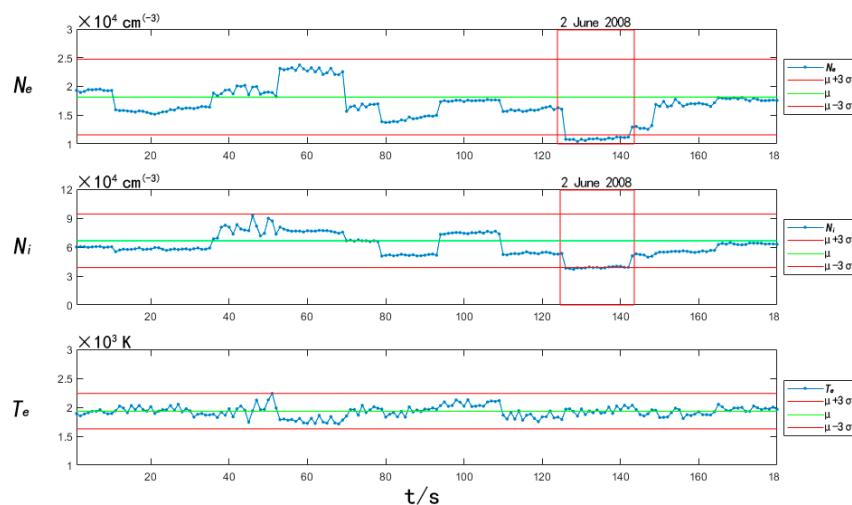

Figure 11. Three-parameter time series plot within anomaly region 1 in seismic example 2.
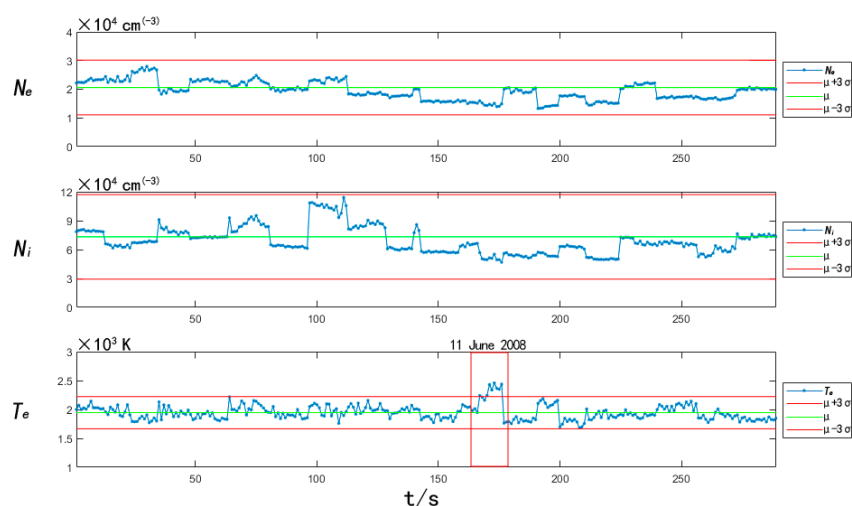

Figure 12. Three-parameter time series plot within anomaly region 2 in seismic example 2.

4.4. Earthquake Example 3

The information on the anomalous region selected for this seismic example is shown in Table 4, and the normalized experimental results are shown in Figure 13.
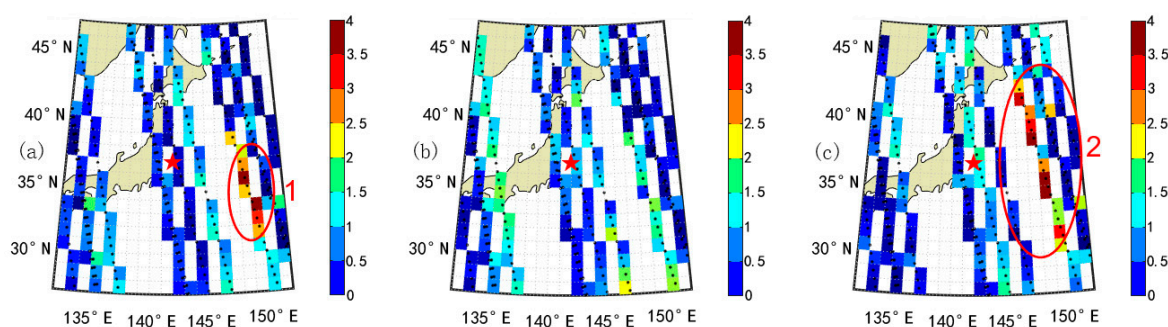
Figure 13. (**a**) Normalized results plot of parameter N_e of earthquake case on 19 July 2008; (**b**) Normalized results plot of parameter N_i of earthquake case on 19 July 2008; (**c**) Normalized results plot of parameter T_e of earthquake case on 19 July 2008.

Table 4. Earthquake case 19 July 2008 anomalous area information.

Region Number	Space Range		Corresponding Orbit	Corresponding Date
	Latitude	Longitude		
1	33–34° N	149–150° E	21592_1	16 July 2008
2	40–41° N	147–148° E	21592_1	16 July 2008

Combining Figures 13–15 shows N_e has an abnormal weakening not only on the third day before the earthquake (16 July 2008) but also on 9 May 2008, and 24 August 2008. Comparing the information of the earthquake cases in Table 1, we can find that the anomalous weakening on 9 May 2008 may be related to the earthquake case on 8 May 2008. Due to the lack of data for the 8 May 2008 example, the case was not studied in depth. We found a strong earthquake with epicenter $(41.8° \text{N}, 144.0° \text{E})$ and magnitude 7.1 occurred in Japan on 11 September 2008. Since this earthquake occurred at a time other than the time interval studied in this paper, this earthquake was not included in the filtered earthquake information. Although the time interval between this phenomenon and the earthquake case is more than 15 days, Ouyang found that the anomaly of N_e reached its maximum 10–20 days before the earthquake [19], so this paper suggests that the anomaly weakened on 24 August 2008, and the earthquake case on 11 September 2008 may be related.
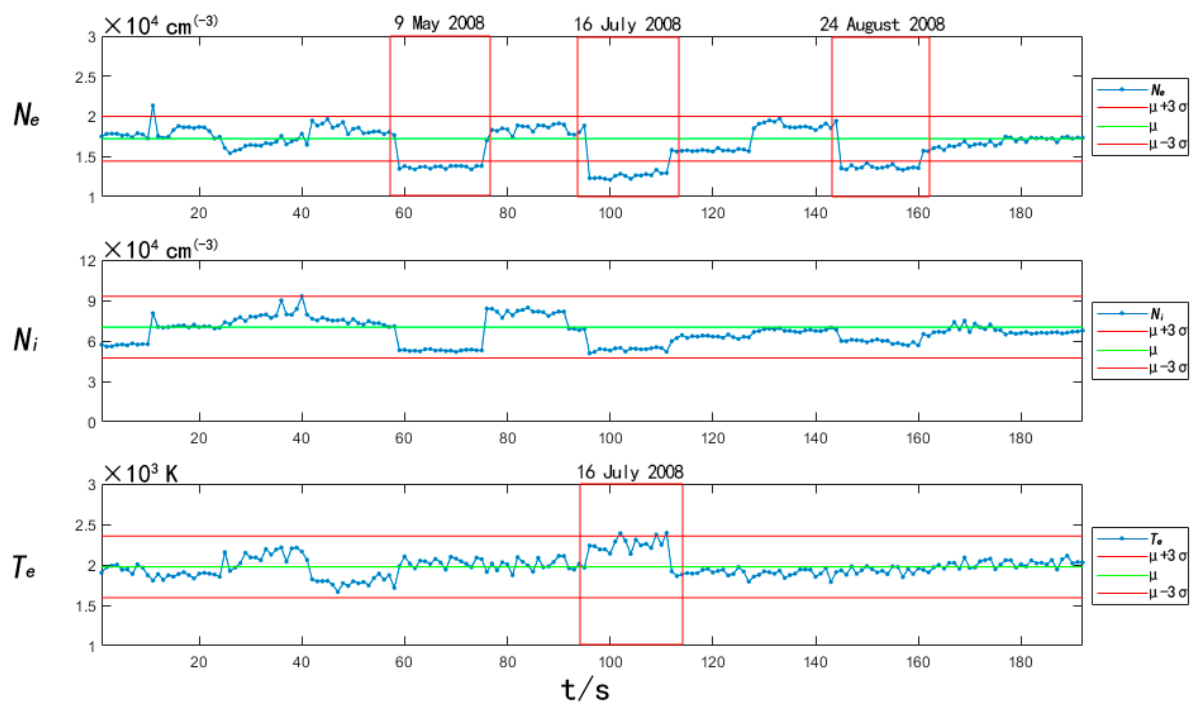

Figure 14. Three-parameter time series plot within anomaly region 1 in seismic example 3.
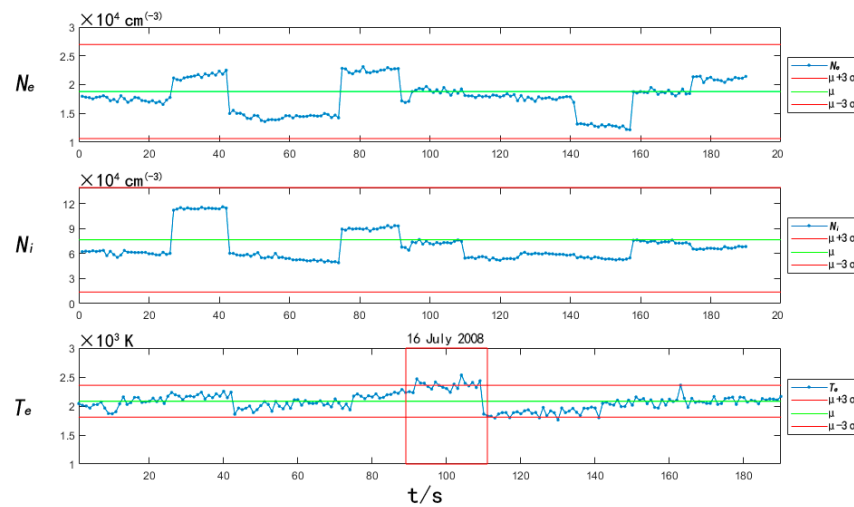
Figure 15. Three-parameter time series plot within anomaly region 2 in seismic example 3.

There was no abnormal phenomenon of N_i in this earthquake case, but the synchronous abnormal phenomenon of N_e and T_e appeared on the third day before the earthquake (16 July 2008), which was manifested in the abnormal weakening of N_e and the abnormal strengthening of T_e.

4.5. Earthquake Example 4

The information on the anomalous region selected for this earthquake example is shown in Table 5, and the normalized experimental results are shown in Figure 16.
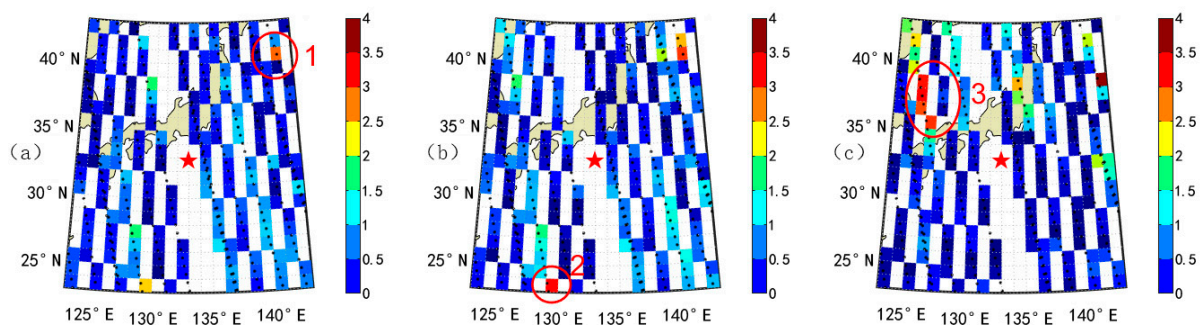

Figure 16. (**a**) Normalized results plot of parameter N_e of earthquake case on 9 August 2009; (**b**) Normalized results plot of parameter N_i of earthquake case on 9 August 2009; (**c**) Normalized results plot of parameter T_e of earthquake case on 9 August 2009.

Table 5. Earthquake case 9 August 2009 anomalous area information.

Region Number	Space Range		Corresponding Orbit	Corresponding Date
	Latitude	Longitude		
1	40–41° N	146–147° E	27146_1	29 July 2009
2	23–24° N	134–135° E	27132_1	28 July 2009
3	38–39° N	130–131° E	27132_1	28 July 2009

Combining Figures 17–19, we can see that on the twelfth day before the earthquake (28 July 2009), there was an anomalous enhancement of T_e in the northwest region of the epicenter, and N_e and N_i also showed an increase, but the intensity of the increase did not exceed 3. There was an anomalous weakening of N_i in the far southwest region of the epicenter; on the eleventh day before the earthquake (29 July 2009), there was a

simultaneous anomalous enhancement of N_e and N_i. The anomalous weakening of N_i on 2 July 2008 was also captured. Since this day was the 18th day after the occurrence of Example 2 and the 17th day before the occurrence of Example 3, whether this anomaly was a post-earthquake effect of Example 2 or a pre-earthquake effect of Example 3 remains to be discussed. These two anomalies may be related to the postseismic effect of this example.
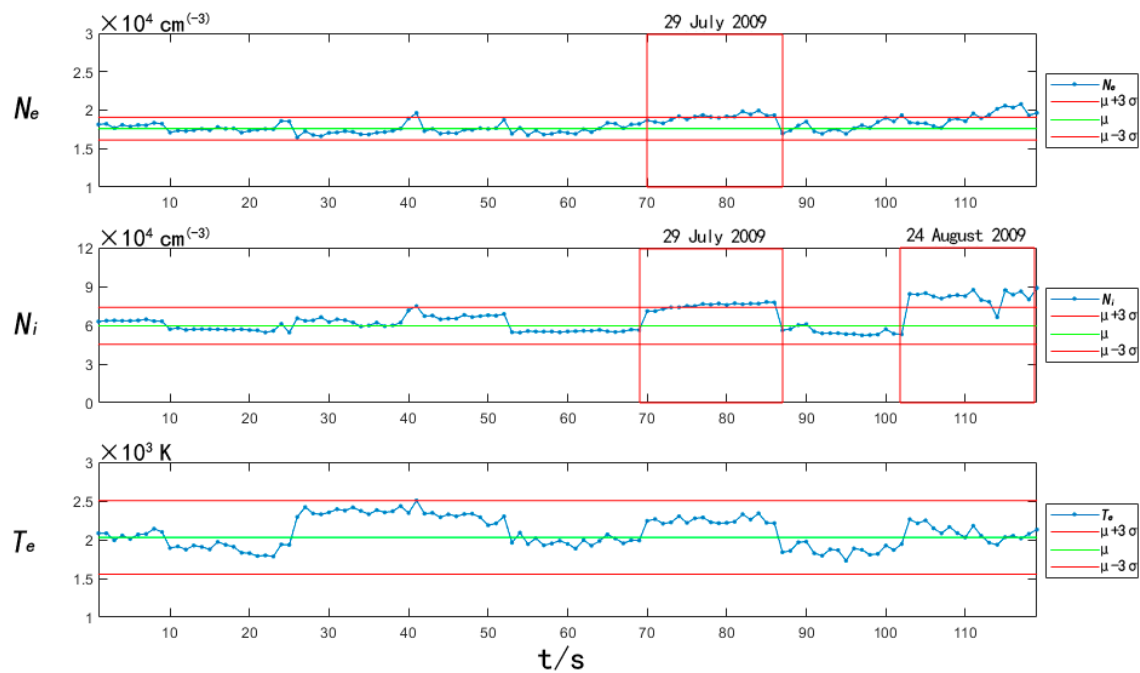

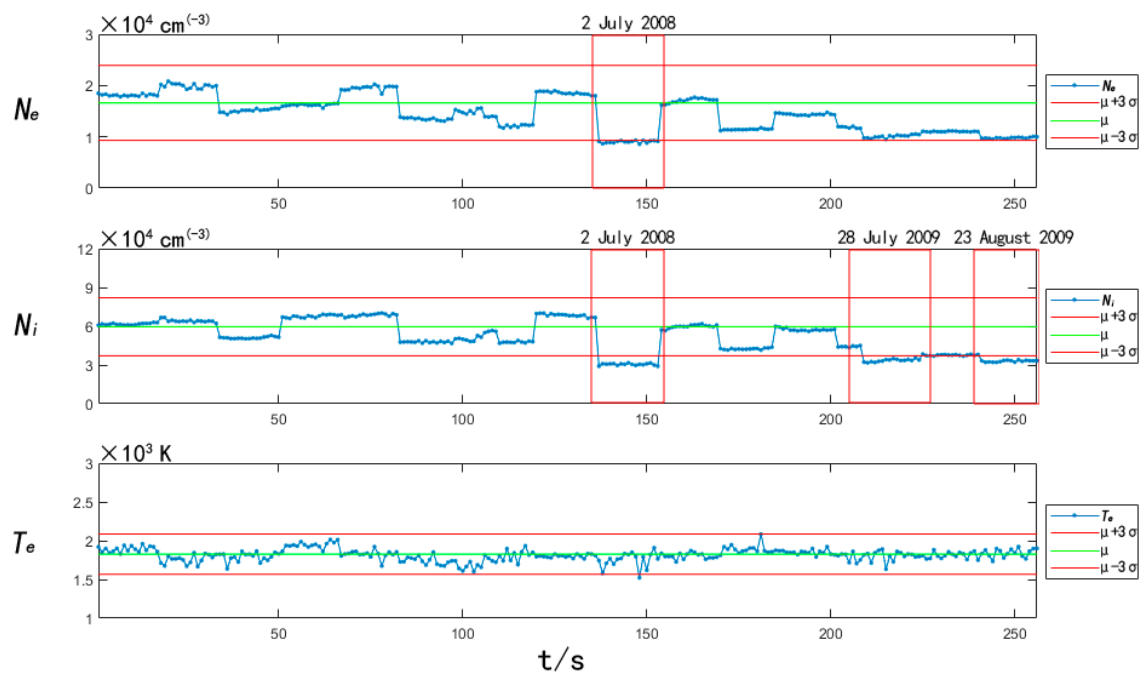**Figure 17.** Three-parameter time series plot within anomaly region 1 in seismic example 4.

Figure 18. Three-parameter time series plot within anomaly region 2 in seismic example 4.
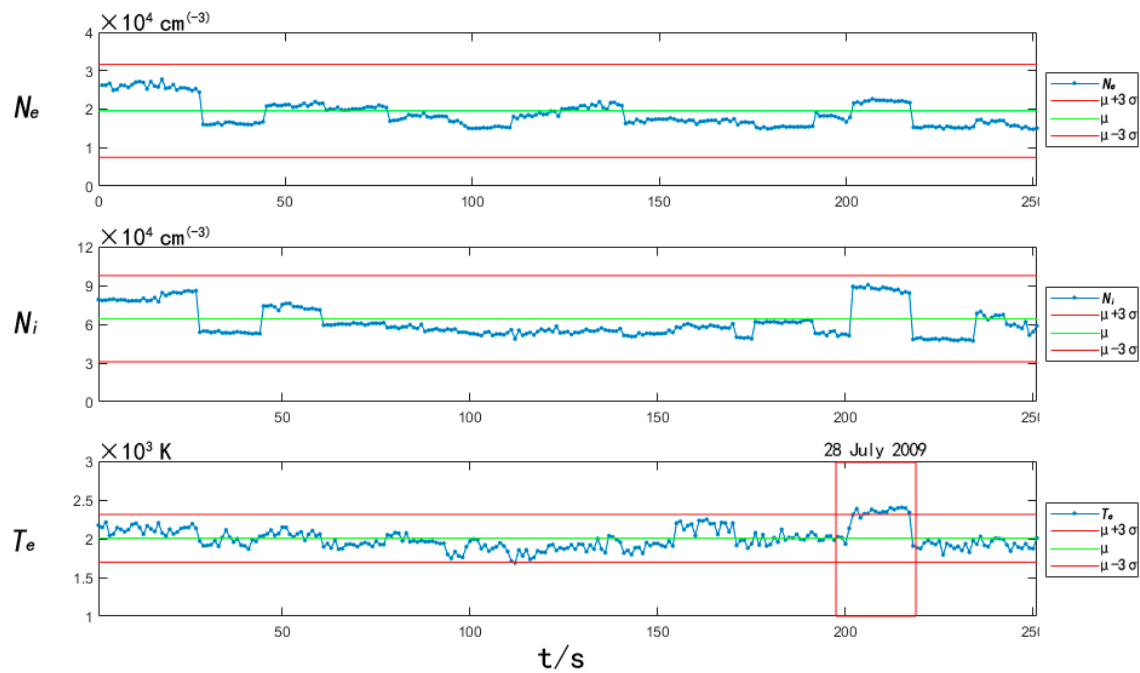
Figure 19. Three-parameter time series plot within anomaly region 3 in seismic example 4.

4.6. Anomalies Collation

From Table 6, we can see that the anomalous enhancement of N_e occurs in the north of the epicenter, which is consistent with the conclusion of He [20] that there is an abnormal increase of N_e in the north of the epicenter during the northern hemisphere seismic events, but there is little mention of the anomalous weakening of N_e in the south of the epicenter. Regarding the time of anomalies before the earthquake, some scholars found that the anomalies occurred 1–7 days before the earthquake [21], and some scholars found that the anomalies started 14 days before the earthquake [22]. In contrast, most of the anomalies obtained in this paper occurred about 9–12 days before the earthquake, so conclusions about the time of earthquake precursors need to be studied in many earthquake cases. Combining the results of this paper and the existing research results, it can be seen that some of the parameters appear to be anomalously enhanced and some appear to be anomalously weakened before the earthquake, and the orientation of the region where the anomalies appear is not fixed relative to the epicenter [5,23]. In response to this phenomenon, there is a mechanism of seismic coupling based on the electrostatic field that rocks are constantly subjected to stress during the gestation process of earthquakes, which activates cavity carriers and leads to the accumulation of positive charges on the earth's surface, thus forming a perturbation electric field E that goes upward from the vertical ground. This perturbation electric field is transmitted to the ionosphere through the atmosphere, and the effect on charged particles in the ionosphere is mainly manifested as a drift phenomenon under the action of $E \times B$. The specific drift direction of charged particles is related to the motion direction of charged particles relative to $E \times B$, which makes the charged particles in the ionosphere anomalously enhanced or anomalously weakened during the earthquake incubation process.

Table 6. Statistical table of earthquake anomalies.

Date	Anomalies					
	N_e		N_i		T_e	
Epicenter	Date and Type of Anomaly	Abnormal Area (Relative to the Epicenter)	Date and Type of Anomaly	Abnormal Area (Relative to the Epicenter)	Date and Type of Anomaly	Abnormal area (Relative to the Epicenter)
16 July 2007 36.7° N, 135.2° E	6 July 2007 Abnormal enhancement	Northwest	6 July 2007 Abnormal enhancement, 7 July 2007 Abnormal enhancement	Northwest and southwest, Southwest	No abnormalities	
14 June 2008 39.1° N, 140.8° E	2 June 2008 Abnormal weakening	Southwest	2 June 2008 Abnormal weakening	Southwest	11 June 2008 Abnormal enhancement	Southeast
19 July 2008 37.5° N,142.3° E	16 July 2008 Abnormal weakening	Southeast	No abnormalities		16 July 2008 Abnormal enhancement	Southeast and southwest
9 August 2009 33.1° N, 138.2° E	29 July 2009 Abnormal enhancement	Northeast	28 July 2009 Abnormal weakening, 29 July 2009 Abnormal enhancement	Southwest, Northeast	28 July 2009 Abnormal enhancement, 29 July 2009 Abnormal enhancement	Northwest, Northeast

5. Conclusions

In this paper, we construct the background ionospheric field over the Japanese region from which we obtain the background variation pattern of the ionosphere and the variation of the indicator t in the absence of earthquakes. Then we capture and study the anomalous phenomena for each earthquake case from both spatial and temporal latitudes. The conclusions obtained are summarized from the following two aspects:

(1) Background characteristics

a. By constructing the background fields of the earthquake cases, it can be seen that N_e, N_i, and T_e all have a variation pattern with increasing latitude, and this pattern is more evident for T_e and the relatively high correlation between N_e and N_i.

b. Most of the nocturnal electron concentration values are distributed between $1 \sim 2 \times 10^4 \text{cm}^{-3}$, most of the ion concentration values are between $4 \sim 8 \times 10^4 \text{cm}^{-3}$, and most of the electron temperature values are between $1 \sim 2 \times 10^3 \text{K}$.

c. In the case of calm and non-seismic space weather, the perturbation intensity of the three-parameter data relative to the background data is around 1, i.e., no anomalies above 3σ occur in the non-seismic case.

(2) Anomalies:

a. In the four cases studied in this paper, N_e showed anomalies exceeding 3σ, three cases showed N_i and T_e anomalies, where N_e and N_i were either anomalously enhanced or weakened before the earthquake, and T_e showed anomalous enhancement.

b. Based on the four earthquake cases, it can be seen that in space, the abnormal enhancement phenomenon of N_e appears in the north of the epicenter, and the abnormal weakening phenomenon appears in the south of the epicenter. The anomalies of N_i and T_e are not significantly related to the orientation. In terms of time, the ionospheric anomalies in the three cases appear 9–12 days before the

earthquake, and the anomaly in Case 3 appears on the third day before the earthquake. By plotting the variation curves of ionospheric parameters with time, we can obtain that the anomalies can still be captured fifteen days before the earthquake in some cases, which indicates to a certain extent that the earthquake incubation time is more than fifteen days. The spatial orientation and time of the anomalies in the cases studied in this paper show that the earthquake precursors in the same area are also diverse.

c. For the analysis of the individual earthquake cases, the time and location of the anomalies of the three parameters have a high consistency, especially the anomalous synchronization of N_e and N_i in the same area simultaneously. Combined with the experimental results under no-earthquake conditions, it is reasonable to suggest that there may be a correlation between the occurrence of these anomalies and earthquake incubation.

The diversity and complexity of many conditions, such as geological structure, source mechanism, and ionospheric influences, make earthquake forecasting still a worldwide problem, and we will study more cases in depth in the future to make the results more convincing.

Author Contributions: Conceptualization, Y.H., Z.Z. and Y.Z.; methodology, J.L.; software, J.L.; formal analysis, J.L.; investigation, J.L.; resources, J.L.; data curation, Y.H.; writing—original draft preparation, J.L.; writing—review and editing, C.J. and Z.M. All authors have read and agreed to the published version of the manuscript.

References

1. Chmyrev, V.M.; Isaev, N.V.; Bilichenko, S.V.; Stanev, G. Observation by space-borne detectors of electric fields and hydromagnetic waves in the ionosphere over an earthquake centre. *Phys. Earth Planet. Inter.* **1989**, *57*, 110–114.
2. Molchanov, O.A.; Mazhaeva, O.A.; Golyavin, A.N.; Hayakawa, M. Observation by the Intercosmos-24 satellite of ELF-VLF electromagnetic emissions associated with earthquakes. *Ann. Geophys.* **1993**, *11*, 431–440.
3. Pulinets, S.A.; Legen'ka, A.D. Spatial-temporal characteristics of the large scale disturbances of electron concentration observed in the F-region of the ionosphere before strong earthquakes. *Cosmic Res.* **2003**, *41*, 221–229.
4. Parrot, M.; Benoist, D.; Berthelier, J.; Błęcki, J.; Chapuis, Y.; Colin, F.; Elie, F.; Fergeau, P.; Lagoutte, D.; Lefeuvre, F.; et al. The magnetic field experiment IMSC and its data processing onboard DEMETER: Scientific objectives, description and first results. *Planet. Space Sci.* **2006**, *54*, 441–455. https://doi.org/10.1016/j.pss.2005.10.015.
5. Yan, X.X.; Shan, X.J.; Cao, J.B.; Tang, J. Statistical analysis of electron density anomalies before global M7.0 earthquakes (2005–2009) using data of DEMETER satellite. *Chin. J. Geophys.* **2014**, *57*, 364–376. https://doi.org/10. 6038/ cjg20140203. (In Chinese)
6. Parrot, M.; Berthelier, J.; Lebreton, J.; Sauvaud, J.; Santolik, O.; Blecki, J. Examples of unusual ionospheric observations made by the DEMETER satellite over seismic regions. *Phys. Chem. Earth Parts A/B/C* **2006**, *31*, 486–495. https://doi.org/10.1016/j.pce.2006.02.011.
7. Zeng, Z.C.; Zhang, B.; Fang, G.Y. The analysis of ionospheric variations before Wenchuan earthquake with DEMETER data. *Chin. J. Geophys.* **2009**, *52*, 11–19. (In Chinese)
8. Xinyan, O.U.; Xuemin, Z.H.; Xuhui, S.H.; Jianping, H.U.; Jing, L.I.; Zhima, Z.E.; Shufan, Z.H. Disturbance of O+ density before major earthquake detected by DEMETER satellite. *Chin. J. Space Sci.* **2011**, *31*, 607–617. (In Chinese)
9. Berthelier, J.; Godefroy, M.; Leblanc, F.; Malingre, M.; Menvielle, M.; Lagoutte, D.; Brochot, J.; Colin, F.; Elie, F.; Legendre, C.; et al. ICE, the electric field experiment on DEMETER. *Planet. Space Sci.* **2006**, *54*, 456–471. https://doi.org/10.1016/j.pss.2005.10.016.
10. Zhang, X.; Shen, X.; Parrot, M.; Zeren, Z.; Ouyang, X.; Liu, J.; Qian, J.; Zhao, S.; Miao, Y. Phenomena of electrostatic perturbations before strong earthquakes (2005–2010) observed on DEMETER. *Nat. Hazards Earth Syst. Sci.* **2012**, *12*, 75–83. https://doi.org/10.5194/nhess-12-75-2012.

11. Yan, R.; Parrot, M.; Pinçon, J.L. Statistical study on variations of the ionospheric ion density observed by DEMETER and related to seismic activities. *J. Geophys. Res. Space Phys.* **2017**, *122*, 12421–12429.

12. Li, M.; Shen, X.; Parrot, M.; Zhang, X.; Zhang, Y.; Yu, C.; Yan, R.; Liu, D.; Lu, H.; Guo, F.; et al. Primary joint statistical seismic influence on ionospheric parameters recorded by the CSES and DEMETER satellites. *J. Geophys. Res. Space Phys.* **2020**, *125*, e2020JA028116.

13. Zheng, L.; Yan, R.; Parrot, M.; Zhu, K.; Zhima, Z.; Liu, D.; Xu, S.; Lv, F.; Shen, X. Statistical Research on Seismo-Ionospheric Ion Density Enhancements Observed via DEMETER. *Atmosphere* **2022**, *13*, 1252.

14. Lebreton, J.P.; Stverak, S.; Travnicek, P.; Maksimovic, M.; Klinge, D.; Merikallio, S.; Lagoutte, D.; Poirier, B.; Blelly, P.L.; Kozacek, Z.M.; et al. The ISL Langmuir probe experiment processing onboard DEMETER: Scientific objectives, description and first results. *Planet Space Sci.* **2006**, *54*, 472–486.

15. Parrot, M.; Mogilevsky, M. VLF emissions associated with earthquakes and observed in the ionosphere and the magnetosphere. *Phys. Earth Planet. Inter.* **1989**, *57*, 86–99. https://doi.org/10.1016/0031-9201(89)90218-5.

16. Sharma, D.K.; Rai, J.; Chand, R.; Israil, M. Effect of seismic activities on ion temperature in the F2 region of the ionosphere. *Atmosfera* **2006**, *19*, 1–7.

17. Dobrovolsky, I.P.; Zubkov, S.I.; Miachkin, V.I. Estimation of the size of earthquake preparation zones. *Pure Appl. Geophys.* **1979**, *117*, 1025–1044. https://doi.org/10.1007/bf00876083.

18. Wang, X.Y.; Yang, D.H.; Chu, W.; Liu, D.P.; Tan, Q.; Li, W.J.; Shen, X.H. Consistency Validation of the Ion Density Data Obtained by the ISL Payload Onboard DEMETER Satellite. *J. Basic Sci. Eng.* **2020**, *28*, 89–102. https://doi.org/10.16058/j.issn.1005-0930.2020.01.009.（in Chinese）

19. Ouyang, X.Y.; Zhang, X.M.; Shen, X.H. Study on ionospheric Ne disturbances before 2007 Puer, Yunnan of China, earthquake. *ActaSeismologica Sin.* **2008**, *30*, 424–436.

20. He, Y.; Yang, D.; Qian, J.; Parrot, M. Response of the ionospheric electron density to different types of seismic events. *Nat. Hazards Earth Syst. Sci.* **2011**, *11*, 2173–2180. https://doi.org/10.5194/nhess-11-2173-2011.

21. Jing, L.; Jianping, H.; Xuemin, Z.; Xuhui, S. Anomaly extraction method study and earthquake case analysis based on in-situ plasma parameters of DEMETER satellite. *ActaSeismologica Sin.* **2013**, *35*, 72–83. (In Chinese)

22. Zhang, X.T.; Tursun, N.L.P.; Xia, C.Y. Study on anomaly of ionospheric electron density before the Yushu earthquake using modified pattern informatics method. *Recent Dev. World Seismol.* **2017**, 19–25. https://doi.org/10.3969/j.issn.0253-4975.2017.10.004.（in Chinese）

23. Liu, J.; Wan, W.X.; Huang, J.P.; Zhang, X.M.; Zhao, S.F.; Ouyang, X.Y.; Zeren, Z.M. Electron density perturbation before Chile M8.8 earthquake. *Chin. J. Geophys.* **2011**, *54*, 2717–2725.